nature geoscience

ARTICLES

https://doi.org/10.1038/s41561-022-01025-x

Climatic and tectonic drivers of late Oligocene Antarctic ice volume

B. Duncan[1]✉, R. McKay[1], R. Levy[1,2], T. Naish[1], J. G. Prebble[2], F. Sangiorgi[3], S. Krishnan[4,10], F. Hoem[3], C. Clowes[2], T. Dunkley Jones[5], E. Gasson[6], C. Kraus[1,11], D. K. Kulhanek[7,12], S. R. Meyers[8], H. Moossen[5,13], C. Warren[4], V. Willmott[9,14], G. T. Ventura[2,15] and J. Bendle[5]

Cenozoic evolution of the Antarctic ice sheets is thought to be driven primarily by long-term changes in radiative forcing, but the tectonic evolution of Antarctica may also have played a substantive role. While deep-sea foraminiferal oxygen isotope records provide a combined measure of global continental ice volume and ocean temperature, they do not provide direct insights into non-radiative influences on Antarctic Ice Sheet dynamics. Here we present an Antarctic compilation of Cenozoic upper-ocean temperature for the Ross Sea and offshore Wilkes Land, generated by membrane lipid distributions from archaea. We find trends of ocean temperature, atmospheric carbon dioxide and oxygen isotopes largely co-vary. However, this relationship is less clear for the late Oligocene, when high-latitude cooling occurred despite interpretation of oxygen isotopes suggesting global warming and ice-volume loss. We propose this retreat of the West Antarctic Ice Sheet occurred in response to a tectonically driven marine transgression, with warm surface waters precluding marine-based ice-sheet growth. Marine ice-sheet expansion occurred only when ocean temperatures further cooled during the Oligocene–Miocene transition, with cold orbital conditions and low atmospheric carbon dioxide. Our results support a threshold response to atmospheric carbon dioxide, below which Antarctica's marine ice sheets grow, and above which ocean warming exacerbates their retreat.

It is well known that the Antarctic Ice Sheet (AIS) is sensitive to multi-millennial-scale variations in Earth's astronomical configuration[1–4]. However, million-year timescale trends in AIS volume are generally controlled by more gradual changes in greenhouse gas concentrations[5], changing continental configurations modulating heat flow towards Antarctica[6] and topographic changes driven by subsidence and erosion on the continent[7,8]. Benthic oxygen isotope ($\delta^{18}O$) records provide critical insights into Cenozoic climate variability[3,9] but are a signal of both deep ocean temperature and global ice-volume change. Additional information from Antarctic-proximal archives is required to fully understand the controls on past AIS dynamics.

Models and near-field geological data indicate the AIS in the Ross Sea region is sensitive to climate forcings such as local insolation, ocean heat flux and local sea-level changes and records variability of both the East Antarctic Ice Sheet (EAIS) and West Antarctic Ice Sheet (WAIS)[1,10–12]. Millions of years of erosion, sedimentation, thermal subsidence and tectonic rifting in the Ross Sea[7,8] have resulted in West Antarctica evolving from an elevated and subaerial region capable of sustaining a large terrestrial ice sheet in the Oligocene[13] to the present-day over-deepened, subsided continental shelf bathymetry occupied by marine-based ice sheets (Fig. 2a)[7,14,15].

In this Article, we investigate the role of climatic and non-climatic drivers in long-term AIS variability by examining the relationship between high-latitude temperature, atmospheric CO_2 and ice volume. We hypothesize that if AIS volume changes were driven directly by radiative forcing and related ocean temperatures, then Southern Ocean sea surface temperatures (SSTs) should largely co-vary with atmospheric CO_2 and benthic $\delta^{18}O$. To test this, we reconstruct Cenozoic upper-ocean temperatures in the Ross Sea and offshore Wilkes Land from a compilation of sediment and outcrop samples (Fig. 1) using glycerol dialkyl glycerol tetraethers (GDGTs), membrane lipids formed by archaea and some bacteria[16] (Supplementary section 1). We apply the recently developed OPTiMAL machine-learning-based temperature calibration to new and legacy GDGT datasets to assign SST estimates (average standard deviation is 3.61 °C) (ref. [17]). We compare these with other GDGT-based temperature calibrations and temperature estimates from fossil assemblages and geochemical datasets at high southern latitudes (Supplementary section 1 and Supplementary Table 1). Compiling a long-term Cenozoic Antarctic-proximal temperature record requires using multiple core sites across a complex glacimarine continental shelf-to-rise depositional transect, influenced by changing water masses and proximity of ocean fronts. This is particularly the case for Integrated Ocean Drilling Program (IODP) Site U1356 on the Wilkes Land continental rise. This site is proximal to the southern boundary of the Antarctic Circumpolar Current (ACC) where glacial–interglacial scale variability is influenced by

[1]Antarctic Research Centre, Victoria University of Wellington, Wellington, New Zealand. [2]GNS Science, Lower Hutt, New Zealand. [3]Department of Earth Sciences, Marine Palynology and Paleoceanography, Utrecht University, Utrecht, the Netherlands. [4]Department of Earth and Planetary Sciences, Yale University, New Haven, CT, USA. [5]School of Geography, Earth and Environmental Sciences, University of Birmingham, Birmingham, UK. [6]Centre for Geography and Environmental Sciences, University of Exeter, Cornwall, UK. [7]International Ocean Discovery Program, Texas A&M University, College Station, TX, USA. [8]Department of Geoscience, University of Wisconsin–Madison, Madison, WI, USA. [9]Department of Marine Organic Biogeochemistry, NIOZ Royal Netherlands Institute for Sea Research, Den Burg (Texel), the Netherlands. [10]Present address: CICERO Center for International Climate and Environmental Research, Oslo, Norway. [11]Present address: Beca Ltd., Wellington, New Zealand. [12]Present address: Institute of Geosciences, Christian-Albrechts-University of Kiel, Kiel, Germany. [13]Present address: Max Planck Institute for Biogeochemistry, Jena, Germany. [14]Present address: International Cooperation Unit, Alfred Wegener Institute, Bremerhaven, Germany. [15]Present address: Department of Geology, Saint Mary's University, Halifax, Nova Scotia, Canada. ✉e-mail: Bella.Duncan@vuw.ac.nz

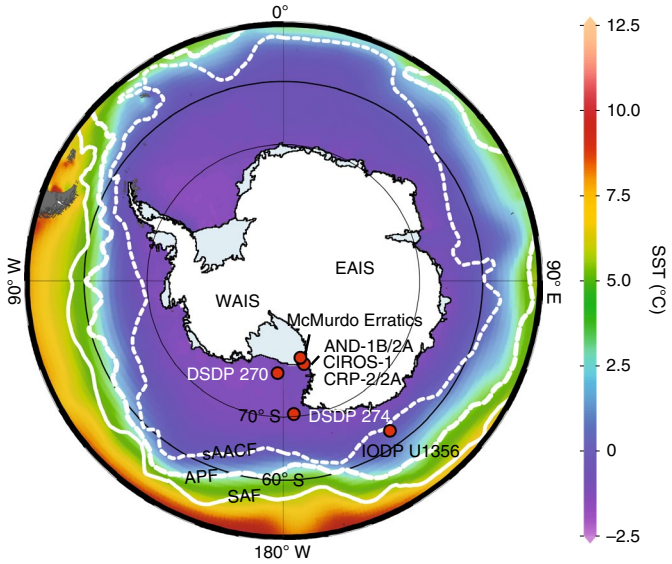

Fig. 1 | Map of the drill core and sample locations used in this study. Annual SSTs[48] and positions of the southern ACC Front (sAACF), Antarctic Polar Front (APF) and Subantarctic Front (SAF)[49] are shown. Plotted using Ocean Data Viewer (https://odv.awi.de).

frontal migration[18,19] (Fig. 1), compared with Ross Sea sites located >14° of latitude farther south (Fig. 1). These caveats are discussed in more detail in Supplementary section 2.

Cenozoic SST compilation

Mid-Eocene (~48–38 million years ago (Ma)) Ross Sea glacial erratics, eroded from subglacial strata and deposited during subsequent ice-sheet advances (Fig. 1 and Methods; palaeolatitude of ~80° S), display highly variable OPTiMAL SSTs (average ~10 °C; maximum values reaching 20 °C), probably reflecting a range of climate states and/or depositional environments over a wide time range (Fig. 2d)[20]. Such values are consistent with temperate terrestrial palynomorph assemblages, shark teeth, mollusc assemblages and a probable crocodile tooth (Supplementary Table 1). Mid and upper Eocene SSTs in the CIROS-1 drill core (Fig. 1 and Extended Data Fig. 1) indicate Ross Sea temperatures were 4.0–6.5 °C by ~36 Ma (Fig. 2d), consistent with a range of qualitative indicators of Southern Ocean cooling and ice growth ~2 million years before widespread AIS expansion across the Eocene–Oligocene Transition (EOT; 34 Ma) (Supplementary Table 1)[21,22]. During the EOT (Fig. 2d), Ross Sea SSTs dropped to as low as 2.4 °C, comparable to mid- to high-latitude Southern Ocean cooling of ~5 °C (ref. [23]). By the early Oligocene, SSTs warmed again, reaching similar values to the late Eocene (~4–6 °C) (Fig. 2), a warming also observed at the Wilkes Land margin (Site U1356; Fig. 1). However, at this more northern site (palaeolatitude of ~59° S), SSTs were notably warmer (reaching 15–20 °C; Fig. 2c), with an ~10–15 °C temperature gradient reflecting the ~14° latitudinal offset (~1,650 km) between sites in our compilation, as well as warmer lower-latitude water masses bathing the Wilkes Land margin before Tasmanian Gateway widening[18].

A substantial latitudinal temperature gradient persisted throughout the Oligocene, although both regions experienced cooling at ~25 Ma (Figs. 2 and 3). Following the Oligocene–Miocene Transition (OMT; ~23 Ma), Ross Sea SSTs in the early Miocene averaged 3 °C (standard deviation of 1.5 °C), with variability probably driven by astronomically paced climate cycles. GDGT-based SSTs in the Ross Sea during the Miocene Climate Optimum (MCO; ~17–15 Ma) average 2.2 °C (standard deviation of 1.5 °C). However, warmer values up to 6–8 °C occur during peak MCO warmth (Fig. 2)[11], comparable to estimates from carbonate clumped isotope (Δ_{47}) analysis and leaf wax isotopes in ANDRILL (AND-) 2A cores (Fig. 1)[11,24], and vegetation assemblages in Transantarctic Mountain lake sediments[25] (Supplementary Table 1). Wilkes Land SSTs remained warmer than the Ross Sea, averaging 7.5 °C, with a larger standard deviation of 3.6 °C (Fig. 2) attributed to warm-water incursions due to weakened Southern Ocean frontal systems that influence Site U1356[19]. The middle Miocene Climate Transition (MMCT; ~14.6–13.8 Ma) is characterized by Ross Sea SSTs averaging ~2.5 °C, but not exceeding 5 °C, although only five samples were examined due to extensive erosion from continental shelf-wide ice-sheet grounding events limiting availability of datable stratigraphic material[11,15]. Across the MMCT, surface cooling and decreasing temperature gradients between Wilkes Land and the Ross Sea probably reflect intensification or southward migration of the Antarctic Divergence proximal to Site U1356 (Fig. 2). Early Pliocene Ross Sea GDGT-based SSTs derived from AND-1B (Fig. 1) averaged ~6 °C, consistent with diatom assemblages and evidence of limited summer sea ice during peak interglacials of the early Pliocene[26]. Such surface temperatures are consistent with mid-Pliocene global mean annual SST reconstructions of 2–3 °C above pre-industrial, assuming ×2–3 polar amplification[27]. The return to warm values similar to the Oligocene and MCO seems surprising at face value, but AND-1B is inherently biased towards interglacial values (Supplementary section 2). In addition, the warmest temperatures in AND-1B occur during the transitions into and out of the peak interglacial intervals, when sedimentary facies and geochemical proxies indicate enhanced glacial meltwater processes and seasonal sea-ice melt, which acts to enhance thermal stratification and warm upper-ocean temperatures[26]. Cold temperatures of 1–3 °C predominantly characterized the late Pliocene–Pleistocene in the Ross Sea (Fig. 2).

Late Oligocene ice-sheet retreat in a cooling climate

Our 46 Myr Ross Sea temperature record shows a trend of ocean cooling in concert with declining atmospheric CO_2 and increasing benthic foraminiferal $\delta^{18}O$ values[3,28,29], implying high-latitude temperature and ice volume are largely coupled over the Cenozoic (Fig. 2). However, this relationship is notably weaker during the late Oligocene (Fig. 3). Following a positive isotope excursion at ~27 Ma (Oi2b event), average $\delta^{18}O$ values then decrease by 0.4–0.6‰ over an ~3 Myr period, a trend widely interpreted as an interval of prolonged global warming[9]. Evidence of circum-Antarctic warm conditions between 27 and 25 Ma include (1) warm-water nannofossil assemblages over Maud Rise and the Kerguelen Plateau[30], (2) Ross Sea dinocyst assemblages and TEX_{86}-based SSTs (Deep Sea Drilling Project (DSDP) Site 274)[31] and (3) dinocyst and sedimentary evidence of limited sea ice and ice-rafted debris from offshore Wilkes Land[32,33]. In the Ross Sea, late Oligocene surface-water temperature data are lacking before 25.5 Ma in DSDP Site 270, with samples between 25.5 and 25.0 Ma recording relatively warm SSTs (~6-7 °C) and diverse foraminifera assemblages with more temperate affinities compared with younger Oligocene assemblages[34].

After ~25 Ma, the deep-sea $\delta^{18}O$ record continues to trend towards lower values, implying warming (Fig. 3), yet our temperature reconstructions show ocean surface cooling in the Ross Sea and Wilkes Land. Palaeoenvironmental proxies also suggest SST cooling and sea-ice cover at this time in the Ross Sea, including nannofossil, marine palynomorph and marine macrofossil assemblages in uppermost Oligocene sediments from Cape Roberts Project (CRP)[35] (Supplementary Table 1). Sedimentary facies analysis and chemical weathering indicators in the CRP and CIROS-1 cores also suggest a minimal change or a long-term cooling trend during the late Oligocene, with conditions periodically cold enough to allow for orbitally paced marine-based EAIS outlet glacier advance into the western Ross Sea (Supplementary Table 1)[4]. Seismic disconformities also indicate Wilkes Land continental shelf marine-based

ice advance occurred after ~25 Ma and are associated with mass transport deposits on the continental rise at IODP Site U1356[33] (Supplementary Table 1).

The contrast of a cooling Antarctic climate from ~25 Ma with inferred warming and/or ice-volume decrease from deep-sea $\delta^{18}O$ records has previously been attributed to reduced proto Antarctic Bottom Water formation and increased warmer, Northern Hemisphere-sourced, deep waters influencing drill sites north of the ACC[36,37]. While this may explain the latitudinal $\delta^{18}O$ gradient, it does not fully explain the trend to lower $\delta^{18}O$ values (reaching a minima at ~24 Ma) in both the Pacific and Atlantic oceans (Fig. 3), especially if the precursor surface waters that form Antarctic Bottom Water in the Ross Sea are cooling as our SST compilation implies. There is also considerable heterogeneity in global SST records over this time[38], with high southern latitudes (discussed here) and equatorial Atlantic records suggesting warming peaked between 26 and 25 Ma, while North and Southwestern Atlantic records show continued warming until 24.0–23.5 Ma (ref. [38]). In the context of these records, we present a hypothesis that reconciles evidence of Antarctic cooling on a background of subsidence-driven ice-sheet retreat in West Antarctica, which we argue provides a mechanism to explain the observed trends in global ocean $\delta^{18}O$ and globally distributed ocean temperature records for the late Oligocene[37,38].

Ice-sheet modelling studies that use restored Antarctic palaeotopographies show a largely subaerial West Antarctica in the Oligocene could accommodate a much larger reservoir of terrestrial ice than today, even with warmer-than-present ocean temperatures in the Ross Sea[7,8,39,40]. Marine-based ice is inherently more sensitive to ocean warming, and retreat is exacerbated by nonlinear processes[39–41]. We suggest that a transgression of relatively warm water across West Antarctica due to tectonic subsidence and glacial erosion drove ocean-induced retreat of the terrestrial WAIS, resulting in a gradual and progressive decrease in ice extent and volume in warmer-than-present late Oligocene climates. The evidence for regional tectonic subsidence comes from a dense network of seismic reflector correlations to DSDP Site 270, for which age control and palaeodepth reconstructions show an extended episode of late Oligocene deepening of the sea floor between ~26 Ma and the early Miocene[7,15,34,42] (Fig. 3). Terrestrial to shallow marine sediments at the base of DSDP site 270 are overlain by mudstones with benthic foraminiferal assemblages indicating water depths of ~200 m between 25.5 and 24.8 Ma, deepening to ~500 m by ~24.5 Ma, with ongoing subsidence continuing after this time (Fig. 3). As the mid-Ross Sea palaeocontinental shelf subsided below sea level, and despite cooling of local SSTs, ocean temperatures remained too warm (Fig. 3) for substantial marine-based ice development, driving a long-term decrease in Antarctic ice volume and contributing to the decreasing trend in global benthic $\delta^{18}O$.

Model experiments show that under constant atmospheric CO_2 concentrations of 500 ppm, changes in bed elevation alone between EOT and OMT topographies can account for an ice-volume difference of 5.7×10^6 km^3 using the 'median' reconstruction of ref. [8] (Methods). Interestingly, a larger, terrestrial WAIS serves to buttress and increase the size of the EAIS, and subsidence-driven retreat in the Ross Sea would also lead to a major loss of the inland EAIS[43]. If most of the subsidence between the EOT and OMT occurred in the late Oligocene, as indicated by seismic data and the DSDP Site 270 reconstructions, then subsidence could account for ice loss equating to an average $\delta^{18}O$ decrease of 0.2‰ (Methods)[39]. However, this example was performed under a constant climate state; feedbacks in the Earth system or orbitally driven climate changes over long periods are not accounted for in this estimate. The total $\delta^{18}O$ decrease from Oi2b at 26.7–24.0 Ma is on the order of 0.4–0.6‰, and it is likely that the earliest phase of this signal was indeed amplified by climate-driven retreat following the warming out of the ~27 Ma Oi2b glacial event[18]. However, following the initiation of cooling in our compilation at ~25 Ma, $\delta^{18}O$ declines by a further ~0.05–0.20‰ (Fig. 3a), which is consistent with continued long-term tectonic-driven retreat. As noted earlier, this signal has previously been explained by heterogeneity in deep-water temperature signals[36,37], and indeed tectonically driven late Oligocene marine AIS retreat could have driven this heterogeneity. Models for the Pliocene show AIS loss in West Antarctica and Wilkes Land acts to slow the ACC and Pacific Ocean overturning circulation, leading to reduced Antarctic Bottom Water formation, increased heat transport to the North Atlantic and divergence of global deep-water mass temperatures in the Pacific and Atlantic oceans[44]. Shifts in ACC circulation and zonal winds relating to contracted AIS volume could also shift surface-water connectivity between the ocean basins and wind-driven upwelling systems[26], contributing to the heterogeneity in global surface-water trends through this time[38].

In summary, we suggest that a continuous decline in average ice-sheet volume occurred between ~27 and 24 Ma. This was probably driven initially by the shift to warmer climatic conditions following the 27 Ma Oi2b glacial event[18], but despite subsequent cooling from ~25 Ma in the Ross Sea and Wilkes Land, the marine sectors of AIS continued to retreat due to basin subsidence and marine incursion across West Antarctica (Fig. 3). Ross Sea SSTs had cooled to ~3 °C by 24.5 Ma, coinciding with a 1.2 Myr node in obliquity, an astronomical configuration favourable to ice-sheet expansion[2]. Proximal glacimarine sedimentary facies were deposited at DSDP Site 270 at this time and mark a period of ice-sheet grounding-line advance into the Ross Sea (Fig. 3)[42,45]. A major increase in obliquity sensitivity (S_{obl}) is also observed at ~24.5 Ma, a metric associated with marine ice-sheet advance and enhanced AIS and ocean connectivity (Fig. 3)[45]. Atmospheric CO_2 records through the Oligocene are sparse, and there is still considerable uncertainty surrounding the absolute values assigned to individual data points, but a clear decline in CO_2 values occurs between the early and late Oligocene (Fig. 2)[5,46]. Pleistocene- to Pliocene-based model–data comparisons[1,8,41] suggest values much lower than 400 ppm (for example, ~280 ppm) are required for marine ice-sheet advance onto the mid-continental shelf of the Ross Sea, while above 400 ppm marine-based ice is absent from West Antarctica and sectors of East Antarctica[41]. Higher-resolution atmospheric proxy CO_2 records, alongside further validation of absolute values, in this critical interval would allow for a better understanding of these thresholds. However, the episode of marine ice-sheet advance at 24.5 Ma was transient and relatively muted in scale in the $\delta^{18}O$ record. Following this, a trend towards a smaller WAIS is reflected by deeper water, ice-distal facies in the latest Oligocene in DSDP Site 270 (Fig. 3)[34,42] and the continued decrease in average deep-sea $\delta^{18}O$ until 24 Ma.

Fig. 2 | SST compilation from Ross Sea and Wilkes Land sample sites. a, Topographic reconstructions. **b**, 1 Myr moving average of benthic $\delta^{18}O$ stack[3]. **c**, OPTiMAL SSTs for Site U1356 Wilkes Land have been recalibrated on the basis of GDGT abundances reported previously[18,19] **d**, OPTiMAL SSTs for Ross Sea sample sites. Vertical error bars in **c** and **d** represent the standard deviation of the temperature estimate (1σ), while horizontal age errors are described in Methods and Supplementary Data Tables 1–3. Samples with $D_{nearest}$ values (a weighted distance metric; see Supplementary section 1) above 0.5 have been removed from the compilations. The black lines represent a 1 Myr moving average. **e**, Atmospheric CO_2 concentrations, with the black line representing a 2 Myr moving average (Methods). Dashed horizontal bars represent atmospheric CO_2 thresholds for a terrestrial AIS[21] and marine AIS[1]. Vertical bars indicate major climate events; E/O, Eocene/Oligocene boundary; O/M, Oligocene/Miocene boundary; NHG, Northern Hemisphere glaciation. Topographic reconstructions from ref. [14] under a Creative Commons license CC BY.

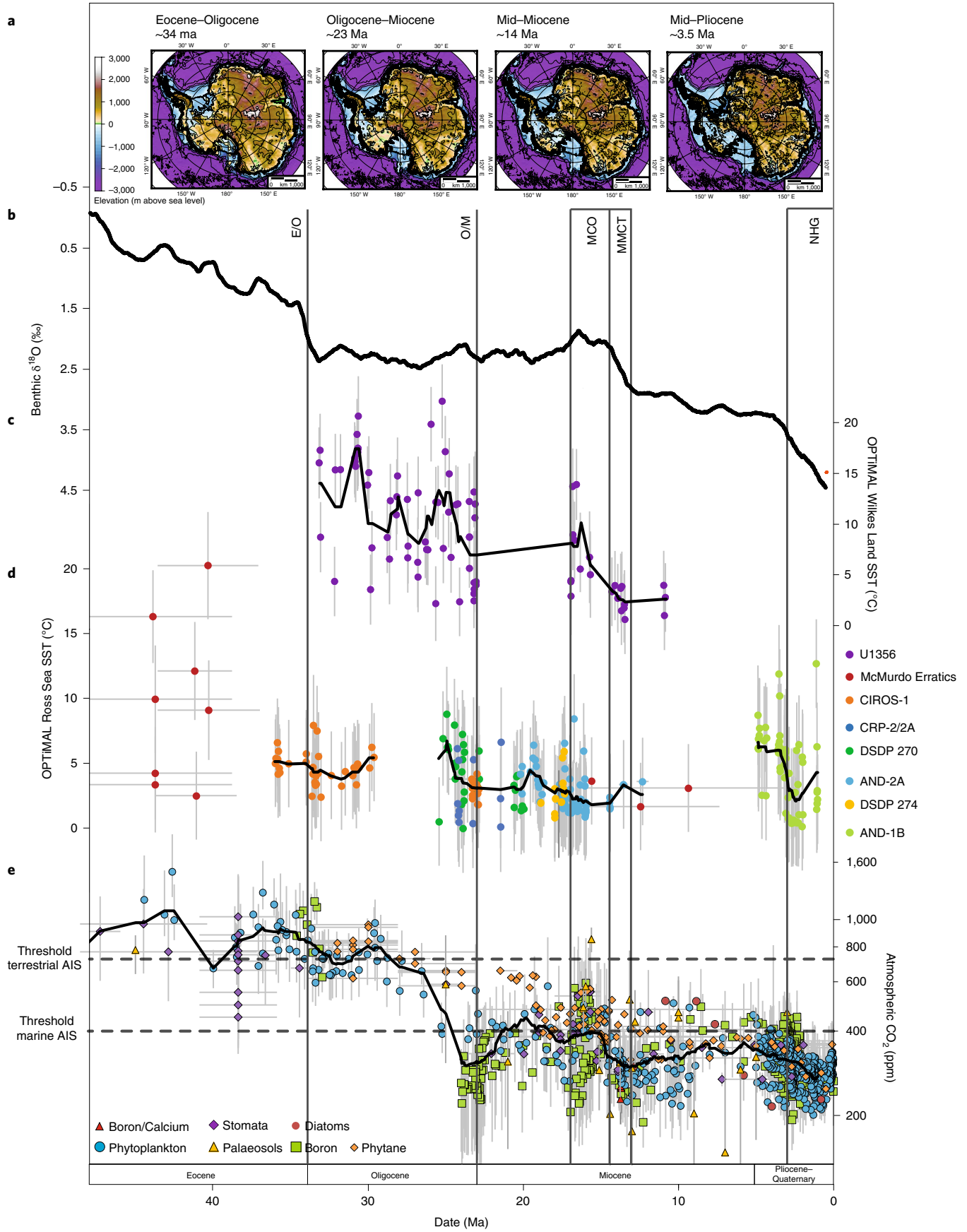
a
Eocene–Oligocene
~34 ma
Oligocene–Miocene
~23 Ma
Mid–Miocene
~14 Ma
Mid–Pliocene
~3.5 Ma
3,000
2,000
1,000
0
−1,000
−2,000
−3,000
Elevation (m above sea level)
b
Benthic δ18O (‰)
E/O
O/M
MCO
MMCT
NHG
c
OPTiMAL Wilkes Land SST (°C)
d
OPTiMAL Ross Sea SST (°C)
U1356
McMurdo Erratics
CIROS-1
CRP-2/2A
DSDP 270
AND-2A
DSDP 274
AND-1B
e
Threshold terrestrial AIS
Threshold marine AIS
Atmospheric CO2 (ppm)
Boron/Calcium
Stomata
Diatoms
Phytoplankton
Palaeosols
Boron
Phytane
Eocene
Oligocene
Miocene
Pliocene–Quaternary
Date (Ma)

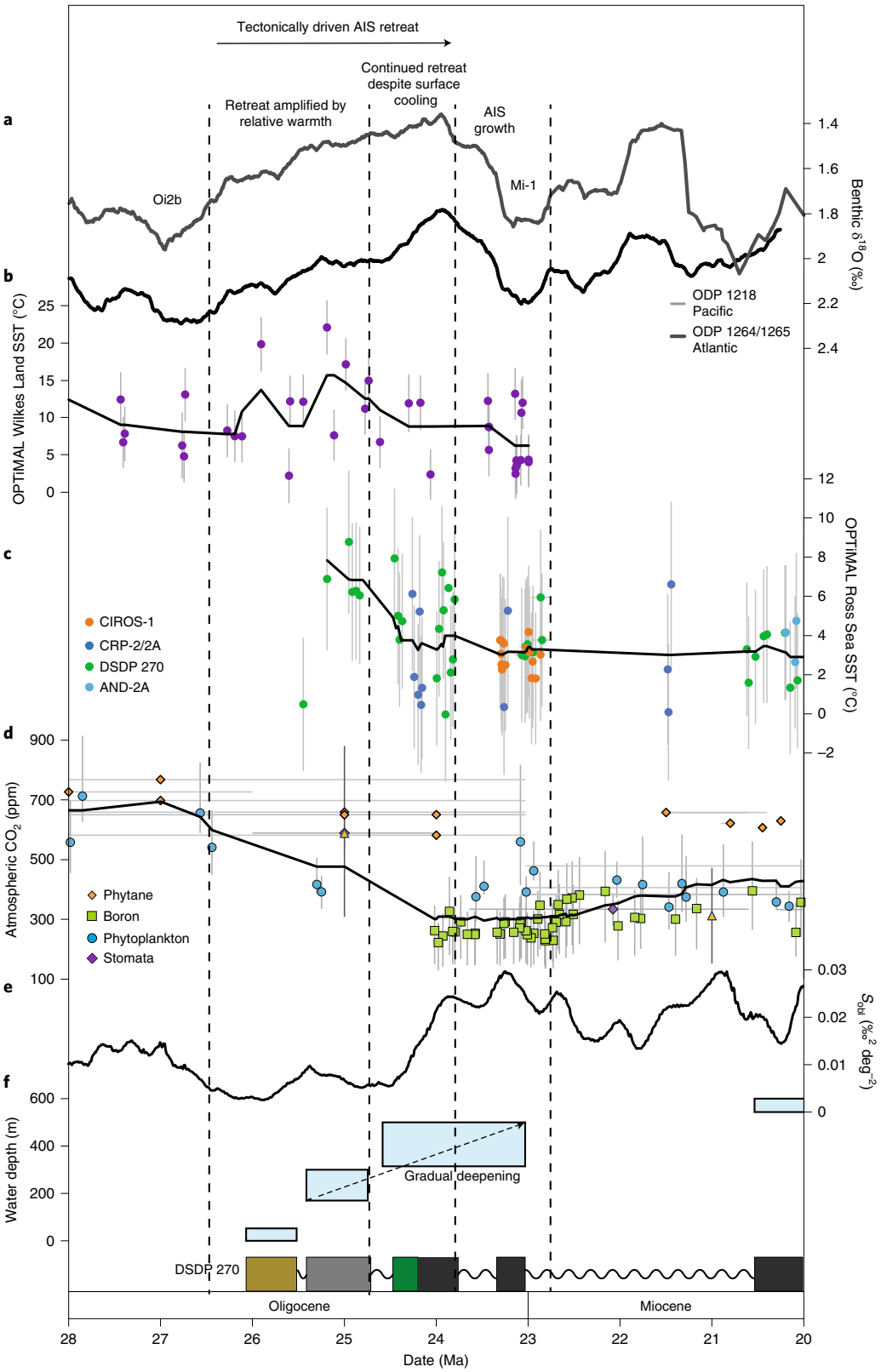

Fig. 3 | Climate indicators across the late Oligocene–early Miocene climate transition. a, 500 kyr moving averages of high-resolution benthic $\delta^{18}O$ records for the late Oligocene from ODP 1218[2] and ODP 1264/1265[50]. **b**, Wilkes Land OPTiMAL temperatures with a 500 kyr moving average in black. **c**, Ross Sea OPTiMAL temperatures with a 500 kyr moving average in black. Vertical error bars for **b** and **c** represent the standard deviation of the temperature estimate (1σ); horizontal age errors are described in Methods and Supplementary Data Tables 1–3. **d**, Atmospheric CO_2 with a 1 myr moving average in black (Methods). **e**, Obliquity sensitivity (S_{obl}) (ref. [45]). **f**, DSDP 270 palaeo water-depth schematic[42], with core log beneath. The light brown on the core log represents an estuarine, shallow marine depositional setting, light grey represents a deepening shelf setting, the green box signifies glacially derived diamictite and dark grey colour represents an outer shelf to deeper marine setting.

After 24 Ma, Ross Sea SSTs continued to cool, crossing a threshold to enable marine-based ice sheets to migrate across the deep continental shelf (Fig. 3). This culminated in the Mi-1 glaciation at 23 Ma, which peaked during a 400 kyr eccentricity minimum and a 1.2 Myr node in obliquity, an optimal configuration for ice growth due to extended low seasonality and cool summer temperatures[2]. Some proxy atmospheric CO_2 reconstructions suggest values reached as low as 265 ppm ($2\sigma^{+166}_{-111}$ ppm) during Mi-1[47]. The Mi-1 event is associated with regional seismic unconformities[15], and major disconformities in DSDP Site 270[42] and CRP-2/2A[4], while $\delta^{18}O$ records indicate it lasted ~200–300 kyr before rebounding in the earliest Miocene towards late Oligocene values. This is consistent with a rapid increase in atmospheric CO_2[47], an astronomical configuration favouring warming and marine-based ice-sheet retreat over the subsided Ross Sea continental shelf. Between 17.8 and 17.4 Ma, SSTs of ~1.5–3.4 °C at AND-2A indicate the threshold for marine-based WAIS advance was again crossed, as evidenced by recent provenance studies from IODP Site U1521 indicating a large WAIS advance resulted in further lowering of elevations in the interior of West Antarctic via glacial erosion[43].

Our compilation of proximal Antarctic temperatures provides climatic constraints on the late Oligocene expansion of marine-based ice sheets, on the background of competing influences on AIS volume resulting from crustal subsidence in West Antarctica. These results are consistent with the concept of a threshold response suggested by previous studies to occur at atmospheric CO_2 values of ~400 ppm[1,10,11,45], above which ocean warming at Antarctica's margin greatly exacerbates marine ice-sheet retreat into interior subglacial basins, with profound consequences for global sea level.

Online content

Any methods, additional references, Nature Research reporting summaries, source data, extended data, supplementary information, acknowledgements, peer review information; details of author contributions and competing interests; and statements of data and code availability are available at https://doi.org/10.1038/s41561-022-01025-x.

Received: 8 December 2020; Accepted: 5 August 2022;
Published online: 15 September 2022

References

1. Naish, T. et al. Obliquity-paced Pliocene West Antarctic Ice Sheet oscillations. *Nature* **458**, 322–328 (2009).
2. Palike, H. et al. The heartbeat of the Oligocene climate system. *Science* **314**, 1894–1898 (2006).
3. Westerhold, T. et al. An astronomically dated record of Earth's climate and its predictability over the last 66 million years. *Science* **369**, 1383–1387 (2020).
4. Naish, T. R. et al. Orbitally induced oscillations in the East Antarctic Ice Sheet at the Oligocene/Miocene boundary. *Nature* **413**, 719–723 (2001).
5. Rae, J. W. B. et al. Atmospheric CO_2 over the past 66 million years from marine archives. *Annu. Rev. Earth Planet. Sci.* **49**, 609–641 (2021).
6. Kennett, J. P. et al. Development of the Circum-Antarctic Current. *Science* **186**, 144–147 (1974).
7. Wilson, D. S. & Luyendyk, B. P. West Antarctic paleotopography estimated at the Eocene–Oligocene climate transition. *Geophys. Res. Lett.* **36**, L16302 (2009).
8. Paxman, G. J. G., Gasson, E. G. W., Jamieson, S. S. R., Bentley, M. J. & Ferraccioli, F. Long-term increase in Antarctic Ice Sheet vulnerability driven by bed topography evolution. *Geophys. Res. Lett.* **47**, e2020GL090003 (2020).
9. Zachos, J., Pagani, M., Sloan, L., Thomas, E. & Billups, K. Trends, rhythms, and aberrations in global climate 65 Ma to present. *Science* **292**, 686–693 (2001).
10. Pollard, D. & DeConto, R. M. Modelling West Antarctic Ice Sheet growth and collapse through the past five million years. *Nature* **458**, 329–332 (2009).
11. Levy, R. et al. Antarctic Ice Sheet sensitivity to atmospheric CO_2 variations in the early to mid-Miocene. *Proc. Natl Acad. Sci. USA* **113**, 3453–3458 (2016).
12. Gomez, N., Weber, M. E., Clark, P. U., Mitrovica, J. X. & Han, H. K. Antarctic ice dynamics amplified by Northern Hemisphere sea-level forcing. *Nature* **587**, 600–604 (2020).
13. Sorlien, C. C. et al. Oligocene development of the West Antarctic Ice Sheet recorded in eastern Ross Sea strata. *Geology* **35**, 467–470 (2007).
14. Paxman, G. J. G. et al. Reconstructions of Antarctic topography since the Eocene–Oligocene boundary. *Palaeogeogr. Palaeoclimatol. Palaeoecol.* **535**, 109346 (2019).
15. De Santis, L., Anderson, J. B., Brancolini, G. & Zayatz, I. in *Geology and Seismic Stratigraphy of the Antarctic Margin* (eds Cooper, A. K. et al.) 235–260 (American Geophysical Union, 1995).
16. Schouten, S., Hopmans, E. C. & Sinninghe Damsté, J. S. The organic geochemistry of glycerol dialkyl glycerol tetraether lipids: a review. *Org. Geochem.* **54**, 19–61 (2013).
17. Dunkley Jones, T. et al. OPTiMAL: a new machine learning approach for GDGT-based palaeothermometry. *Climate* **16**, 2599–2617 (2020).
18. Hartman, J. D. et al. Paleoceanography and ice sheet variability offshore Wilkes Land, Antarctica—part 3: insights from Oligocene–Miocene TEX_{86}-based sea surface temperature reconstructions. *Climate* **14**, 1275–1297 (2018).
19. Sangiorgi, F. et al. Southern Ocean warming and Wilkes Land ice sheet retreat during the mid-Miocene. *Nat. Commun.* **9**, 317 (2018).
20. Stilwell, J. D. & Feldmann, R. M. *Paleobiology and Paleoenvironments of Eocene Rocks: McMurdo Sound, East Antarctica* (American Geophysical Union, 2000).
21. Galeotti, S. et al. Antarctic Ice Sheet variability across the Eocene–Oligocene boundary climate transition. *Science* **352**, 76–80 (2016).
22. Carter, A., Riley, T. R., Hillenbrand, C.-D. & Rittner, M. Widespread Antarctic glaciation during the late Eocene. *Earth Planet. Sci. Lett.* **458**, 49–57 (2017).
23. Liu, Z. et al. Global cooling during the Eocene–Oligocene Climate Transition. *Science* **323**, 1187–1190 (2009).
24. Feakins, S. J., Warny, S. & Lee, J.-E. Hydrologic cycling over Antarctica during the middle Miocene warming. *Nat. Geosci.* **5**, 557–560 (2012).
25. Lewis, A. R. & Ashworth, A. C. An early to middle Miocene record of ice-sheet and landscape evolution from the Friis Hills, Antarctica. *GSA Bull.* **128**, 719–738 (2016).
26. McKay, R. et al. Antarctic and Southern Ocean influences on late Pliocene global cooling. *Proc. Natl Acad. Sci. USA* **109**, 6423–6428 (2012).
27. Haywood, A. M. et al. Large-scale features of Pliocene climate: results from the Pliocene Model Intercomparison Project. *Clim. Past* **9**, 191–209 (2013).
28. Cramer, B. S., Toggweiler, J. R., Wright, J. D., Katz, M. E. & Miller, K. G. Ocean overturning since the late cretaceous: inferences from a new benthic foraminiferal isotope compilation. *Paleoceanography* **24** (2009).
29. Miller, K. G. et al. Cenozoic sea-level and cryospheric evolution from deep-sea geochemical and continental margin records. *Sci. Adv.* **6**, eaaz1346 (2020).
30. Villa, G., Fioroni, C., Persico, D., Roberts, A. P. & Florindo, F. Middle Eocene to late Oligocene Antarctic glaciation/deglaciation and Southern Ocean productivity. *Paleoceanography* **29**, 223–237 (2014).
31. Hoem, F. S. et al. Temperate Oligocene surface ocean conditions offshore of Cape Adare, Ross Sea, Antarctica. *Clim. Past* **17**, 1423–1442 (2021).
32. Bijl, P. K. et al. Paleoceanography and ice sheet variability offshore Wilkes Land, Antarctica—part 2: insights from Oligocene–Miocene dinoflagellate cyst assemblages. *Clim. Past* **14**, 1015–1033 (2018).
33. Salabarnada, A. et al. Paleoceanography and ice sheet variability offshore Wilkes Land, Antarctica—part 1: insights from late Oligocene astronomically paced contourite sedimentation. *Clim. Past* **14**, 991–1014 (2018).
34. Leckie, R. M. & Webb, P.-N. Late Oligocene–early Miocene glacial record of the Ross Sea, Antarctica: evidence from DSDP Site 270. *Geology* **11**, 578–582 (1983).
35. Barrett, P. J. in *Glacial Sedimentary Processes and Products* (eds Hambrey, M. J. et al.) 259–287 (Blackwell, 2007).
36. Pekar, S. F., DeConto, R. M. & Harwood, D. M. Resolving a late Oligocene conundrum: deep-sea warming and Antarctic glaciation. *Palaeogeogr. Palaeoclimatol. Palaeoecol.* **231**, 29–40 (2006).
37. Hauptvogel, D. W., Pekar, S. F. & Pincay, V. Evidence for a heavily glaciated Antarctica during the late Oligocene "warming" (27.8–24.5 Ma): stable isotope records from ODP Site 690. *Paleoceanography* **32**, 384–396 (2017).
38. O'Brien, C. L. et al. The enigma of Oligocene climate and global surface temperature evolution. *Proc. Natl Acad. Sci. USA* **117**, 25302–25309 (2020).
39. Gasson, E., DeConto, R. M., Pollard, D. & Levy, R. H. Dynamic Antarctic Ice Sheet during the early to mid-Miocene. *Proc. Natl Acad. Sci. USA* **113**, 3459–3464 (2016).
40. Colleoni, F. et al. Past continental shelf evolution increased Antarctic Ice Sheet sensitivity to climatic conditions. *Sci Rep.* **8**, 11323 (2018).
41. DeConto, R. M. & Pollard, D. Contribution of Antarctica to past and future sea-level rise. *Nature* **531**, 591–597 (2016).
42. Kulhanek, D. K. et al. Revised chronostratigraphy of DSDP Site 270 and late Oligocene to early Miocene paleoecology of the Ross Sea sector of Antarctica. *Glob. Planet. Change* **178**, 46–64 (2019).

43. Marschalek, J. W. et al. A large West Antarctic Ice Sheet explains early Neogene sea-level amplitude. *Nature* **600**, 450–455 (2021).
44. Hill, D. J., Bolton, K. P. & Haywood, A. M. Modelled ocean changes at the Plio-Pleistocene transition driven by Antarctic ice advance. *Nat. Commun.* **8**, 14376 (2017).
45. Levy, R. H. et al. Antarctic ice-sheet sensitivity to obliquity forcing enhanced through ocean connections. *Nat. Geosci.* **12**, 132–137 (2019).
46. Foster, G. L., Royer, D. L. & Lunt, D. J. Future climate forcing potentially without precedent in the last 420 million years. *Nat. Commun.* **8**, 14845 (2017).
47. Greenop, R. et al. Orbital forcing, ice volume, and CO_2 across the Oligocene–Miocene Transition. *Paleoceanogr. Paleoclimatology* **34**, 316–328 (2019).
48. Locarnini, M. M. et al. *World Ocean Atlas 2018, Volume 1: Temperature* (2018).
49. Orsi, A. H., Whitworth, T. & Nowlin, W. D. On the meridional extent and fronts of the Antarctic Circumpolar Current. *Deep Sea Res. Part 1* **42**, 641–673 (1995).
50. Liebrand, D. et al. Cyclostratigraphy and eccentricity tuning of the early Oligocene through early Miocene (30.1–17.1 Ma): *Cibicides mundulus* stable oxygen and carbon isotope records from Walvis Ridge Site 1264. *Earth Planet. Sci. Lett.* **450**, 392–405 (2016).

Methods

Sampling sites and age models. Proximal Antarctic cores contain frequent unconformities, which are often the product of ice-sheet overriding or other erosional processes in a glacimarine environment. To compile a long-term Cenozoic record of ocean temperatures from the Ross Sea required using multiple sampling sites and core sites from across the region (Fig. 1). We present data from the McMurdo Erratics, CIROS-1, DSDP 270, CRP-2A and DSDP 274 and compile this with previously published data from AND-1B and 2A. Age models have been developed using published age datums (Supplementary Data Table 3), but to ensure a consistent approach for assigning ages to core depths between datums, we use the Bayesian age–depth modelling functionality in the R package Bchron (Supplementary Data Table 3)[51]. The sites included in the Ross Sea compilation are detailed in the following. We have compared our Ross Sea compilation with a previously published dataset from IODP U1356, offshore the Wilkes Land margin, with GDGT abundances, age model and lithologies[18,33,52].

McMurdo Erratics. The oldest sediments used in this compilation are glacial erratics, collected from the Mount Discovery and Minna Bluff region (Fig. 1)[53]. The erratics have been eroded from sediments deposited in sub-ice basins in the western Ross Sea associated with early Cenozoic rifting during Gondwanaland break-up. These rift-fill sediments were subsequently eroded (probably from the Discovery Deep region) and transported to surficial morainal deposits by expanded ice sheets during past glacial periods. The erratics sampled in this study were deposited in coastal–terrestrial and nearshore marine environments[53]. Ages for the erratics from the volumes in ref. [53] have been updated to most recent ages for the described taxa (Supplementary Data Table 2).

CIROS-1. The CIROS-1 core was drilled in McMurdo Sound in 1986 (Fig. 1)[54]. The upper part of the core (366–0 metres below sea floor (mbsf)) is glacially influenced, with major glacial advances represented by massive and stratified diamictites[55]. Below an unconformity, the lower sequence of the core (702–366 mbsf) displays substantially less subglacial influence, containing marine mudstones and sandstones but with ice-rafted debris indicating the presence of marine-terminating glaciers at the coastline[55]. The upper part of the core is late Oligocene/early Miocene in age[56]. Age control for the lower part of the CIROS-1 core has undergone a series of revisions since recovery in 1986[57–59]. Our age model for the Eocene/Oligocene boundary interval is an improvement on previous attempts as we incorporate new observations of dinoflagellate cysts with occurrences recently described in other Antarctic and Southern Ocean cores[52,60–62]. These new observations allow precise constraint of the updated palaeomagnetic record[59] of the geomagnetic polarity timescale[63]. In addition, we include updated range data to constrain the ages of biostratigraphic events previously identified in the core. Microfossil reworking has long been recognized as a major problem in the glacial sediments of Antarctica[64–66]. In constructing our age model, we have given preference to ensuring conformity to biostratigraphic first occurrences and are much less concerned about apparent last occurrences in this setting. In addition to the biochronologic controls, we include new $^{87}Sr/^{86}Sr$ isotope ratio ages from disarticulated bivalves between 460 and 470 mbsf in the core. Measurements were undertaken at the CSIRO laboratory in Sydney. These ages are interpreted to represent minimum ages.

Biostratigraphic datums are shown in Supplementary Data Table 1, the age–depth chart is in Extended Data Fig. 1 and tie points of Age Model 1 used for linear extrapolation of environmental proxies are in Supplementary Data Table 3. Four age models were explored; Model 1 is preferred. Model 1 and Model 2 minimize inconsistency with biostratigraphic first occurrences, place the Eocene/Oligocene boundary at 547 mbsf and assign the interval of normal polarity between 435 and 503 mbsf to Chron C13n. Model 1 and Model 2 place different priority on inconsistencies with biostratigraphic last occurrences and the robustness of intervals of magnetic reversals constrained by only a few observations. Model 1 minimizes inconsistencies with the geomagnetic polarity record but does not seek to minimize biostratigraphic last occurrences. By contrast, Model 2 requires that the intervals of normal polarity at 408 m and 421 mbsf, constrained by only one and two measurements of magnetic polarity, respectively[59], are a transient, local signal not reflective of the global magnetic field. Models 3 and 4 explore the possibility that the interval of normal polarity between 435 and 503 mbsf is Chron C15n (Model 3) or Chron C12n (Model 4). Model 3 is the most unlikely as it contains seven inconsistencies with biostratigraphic first occurrences across four fossil groups. Model 4 is consistent with the palaeomagnetic record and the biostratigraphic first occurrences but is inconsistent with every available biostratigraphic last occurrence. It would also require a pronounced increase in the proportion of protoperidinioid dinoflagellate cysts observed between 495 and 530 mbsf to have occurred more than 2 Myr later than observed in other circum-Antarctic cores[62].

One perplexing aspect of the CIROS-1 biostratigraphy is the virtual absence of the dinoflagellate cyst *Malvinia escutiana*, which has a first occurrence in the earliest Oligocene in other Southern Ocean records[61]. A single specimen of *M. escutiana* was recorded in CIROS-1, at 376.39 mbsf, within Subchron C11n.2n of age Model 1 (this study). *M. escutiana* has been identified in the nearby CRP-3 core[62]. Those authors do not report their count data for their CRP-3 dinoflagellate cysts but note that specimens of *M. escutiana* were recorded somewhere in the interval between 13.4 and 151.97 mbsf. Following the age model for CRP-3 (Age Model 3[67]), this would place the CRP-3 occurrences of *M. escutiana* within Chron C12n to upper C12r. This suggests *M. escutiana* may not have a major presence in the Ross Sea in the earliest Oligocene, in contrast to observations on the Wilkes Land margin at IODP Site U1356[52,62].

DSDP 270. The DSDP Site 270 was recovered from the Eastern Basin of the central Ross Sea in 1973 (Fig. 1)[68]. This core records a deepening sequence of glacimarine sediments, represented by glacimarine mudstones, interstratified mudstones and sandstones and massive and stratified diamictites[34,42,68]. Samples for this study have been taken from glacimarine sediments between 387.9 and 27.8 mbsf, dated as late Oligocene to early Miocene[42].

CRP-2/2A. The Cape Roberts Project recovered CRP-2/2 A off the Victoria Land coast of Antarctica in 1999 (Fig. 1)[35]. Samples have been taken from three glacimarine sediment sequences in the upper Oligocene–lower Miocene section of the core, recording the expansion and contraction of the EAIS[69,70].

AND-2A. The AND-2A core was recovered in 2007 from Southern McMurdo Sound as part of the ANDRILL programme (Fig. 1)[11]. Samples for this compilation were collected from the lower Miocene to mid-Miocene section of the core and were published as TEX^{L}_{86} values[11], calibrated to ref. [71] (Supplementary Data Table 4). Glacimarine sediments through this section represent ice-distal to ice-proximal and occasionally subglacial settings, reflecting advance and retreat of grounded ice across the drill site[72,73].

DSDP 274. The DSDP Site 274 was drilled on the lower continental rise in the northwestern Ross Sea in 1973 (Fig. 1)[68]. Samples for this study were taken from middle Miocene diatom-rich silty clay at 156–142 mbsf. Ages have been assigned using the relaxed hybrid CONOP model of ref. [74] (Supplementary Data Table 3). This model does not extend below 141.26 mbsf. For samples below this depth, the same linear sedimentation rate that occurs above 141.26 mbsf is used. This is constrained by the first appearance of *Denticulopsis maccollumii* at 141.26 mbsf (dated to 17.05 Ma) and the first appearance of *Actinocyclus ingens* at 113.6 mbsf (dated to 15.83 Ma). The continuation of this sedimentation rate is supported by the apparent lack of a hiatus or change in lithology through this interval[68].

AND-1B. The AND-IB core was drilled in 2006 as part of the ANDRILL McMurdo Ice Shelf Project (Fig. 1), and samples were compiled from published data from the Plio–Pleistocene section of the core[1] (Supplementary Data Table 4). Pliocene sediments reflect successions of advance and retreat of the marine-based ice sheet in the Ross Sea and consist of cycles of diamictite, mudstone and diatomite bounded by glacial erosion surfaces[26].

GDGT processing and analysis. Samples from DSDP 270, CRP-2/2 A and DSDP 274 were processed for GDGTs at the Birmingham Molecular Climatology Laboratory, University of Birmingham. Lipids were extracted from ~10–15 g homogenized sediment by ultrasonic extraction using dichloromethane (DCM)/methanol (3/1). The total lipid extract was fractionated by silica gel chromatography using n-hexane, n-hexane/DCM (2/1), DCM and methanol to produce four separate fractions, the last of which contained the GDGTs. Procedural blanks were also analysed to ensure the absence of laboratory contaminants.

Samples were filtered using hexane/isopropanol (99/1) through a 0.4 µm polytetrafluroethylene filter (Alltech part 2395) before being dried under a continuous stream of N_2. Samples were then sent to Yale University for analysis. Samples were redissolved in hexane/isopropanol (99/1) and analysed and quantified on an Agilent single quadrupole liquid chromatography mass spectrometer 6100 series using previously established protocols[75]. Due to frequent low abundances of compounds, some samples were re-run at higher concentrations, and integrations derived from these re-runs were favoured. Samples were integrated multiple times and averaged to account for potential integration variation, with an average TEX_{86} standard deviation of 0.007 between integrations. The areas of individual GDGTs as well as calculated indices and temperature calibrations are recorded in Supplementary Data Table 4.

Methodology for samples from AND-1B and AND-2A are described in previous works[11,26]. Unpublished results for samples from CIROS-1 and the McMurdo Erratics were processed and analysed at NIOZ using methods outlined in ref. [75]. Another four previously unpublished results for samples from DSDP 274 (depths 153.63 mbsf, 155.68 mbsf, 163.75 mbsf and 174.2 mbsf) were also added to the compilation. These were extracted using an accelerated solvent extractor and then fractionated by Al_2O_3 column chromatography using hexane/DCM (9/1, v/v), hexane/DCM (1/1) and DCM/MeOH (1/1). The samples were then dissolved in hexane/isopropanol (99/1, v/v) and filtered over a 0.45 µm polytetrafluoroethylene filter before being analysed following procedures outlined in ref. [76] As samples were processed at three different laboratory facilities (University of Birmingham, Yale University and NIOZ) and analysed between two facilities (Yale University and NIOZ), the potential for interlaboratory biases must be considered. Previously reported results from a comparison of 35 laboratories found that TEX_{86} and BIT indices were not significantly affected by differences in sediment extraction

and processing techniques[77]. TEX_{86} measurements had an interlaboratory reproducibility for different samples ranging from 0.023 to 0.053, with the differences suggested to be due to instrumental characteristics. The BIT index was found to have good reproducibility at the extremes of the index, where values were close to either 0 or 1, but poorer reproducibility for intermediate values, with values typically overestimated. Samples from AND-1B were processed and analysed at both Yale University and NIOZ. Chromatograms of samples analysed in each laboratory were integrated by members of the other for comparison and were found to have an average SST difference of ±0.8 °C, when the TEX^{L}_{86} calibration[78] was used[26]. Four samples processed at Yale University were also analysed at NIOZ, with an average SST difference of 0.8 °C (ref. [26]). The results discussed suggest that while some interlaboratory differences are possible, they probably have a minor influence on reported SST values[26,77].

CO_2 compilation. The compilation of atmospheric CO_2 concentrations is based on previous compilations[47,79,80], but updated with more recent datasets, and individual sample errors are described in refs. [47,80–86]. One outlier value of 2,622 ppm has been removed at 36.48 Ma. Moving averages for CO_2 and temperature datasets were derived using mwStats in the R package astrochron[87].

Ice-sheet model. Modelling sensitivity tests have previously demonstrated large ice-volume differences can result solely from changing topographic boundary conditions through time[8,39,40,88]. To assess the potential impact topographic changes between the EOT and OMT may have had on oxygen isotope shifts in deep-sea records, we expanded on previous ice-sheet modelling experiments of Paxman et al.[8] by rerunning selected experiments with an isotope-enabled ice-sheet model[89]. Experiments run under a steady-state climate with an atmospheric CO_2 concentration of 500 ppm and an imposed 5 °C warming of the ocean relative to present show a larger AIS (34.6×10^6 km^3) was in place with an EOT topography relative to experiments with the same climate and an OMT topography, which had a greatly reduced ice volume (28.9×10^6 km^3), with most of this change occurring in the WAIS. Our isotope-enabled simulations suggest that due solely to changes in topography, there would have been a shift in the oxygen isotope composition of seawater of 0.2‰. These experiments did not include the marine ice-cliff instability[41] and were chosen as they demonstrated the greatest sensitivity to topographic change with the chosen climate forcing. Although beyond the scope of this study, we expect that at a lower atmospheric CO_2 forcing and ocean warming, there would be comparable (or greater) sensitivity to changes to topography in experiments including the marine ice-cliff instability.

Data availability

Datasets generated during and/or analysed during the current study are available in Supplementary Data Tables 1–4 and online at https://doi.org/10.1594/PANGAEA.94680189[90].

References

51. Haslett, J. & Parnell, A. A simple monotone process with application to radiocarbon-dated depth chronologies. *J. R. Stat. Soc. Ser. C* **57**, 399–418 (2008).
52. Bijl, P. K., Houben, A. J. P., Bruls, A., Pross, J. & Sangiorgi, F. Stratigraphic calibration of Oligocene–Miocene organic-walled dinoflagellate cysts from offshore Wilkes Land, East Antarctica, and a zonation proposal. *J. Micropalaeontol.* **37**, 105–138 (2018).
53. Harwood, D. M. & Levy, R. H. in *Paleobiology and Paleoenvironments of Eocene Rocks: McMurdo Sound, East Antarctica* (eds Stilwel, J. D. & Feldman, R. M.) 1–18 (American Geophysical Union, 2000).
54. Barrett, P. J. (ed) *Antarctic Cenozoic History from the CIROS-1 Drillhole, McMurdo Sound* (DSIR, 1989).
55. Hambrey, M. J., Barrett, P. J. & Robinson, P. H. in *Antarctic Cenozoic History from the CIROS-1 Drillhole, McMurdo Sound* (ed. Barrett, P. J.) 23–48 (DSIR, 1989).
56. Roberts, A. P., Wilson, G. S., Harwood, D. M. & Verosub, K. L. Glaciation across the Oligocene–Miocene boundary in southern McMurdo Sound, Antarctica: new chronology from the CIROS-1 drill hole. *Palaeogeogr. Palaeoclimatol. Palaeoecol.* **198**, 113–130 (2003).
57. Coccioni, R. & Galeotti, S. Foraminiferal biostratigraphy and palaeoecology of the CIROS-1 core from McMurdo Sound (Ross Sea, Antarctica). *Terra Antarctica* **4**, 103–117 (1997).
58. Hannah, M. J. Climate controlled dinoflagellate distribution in late Eocene–earliest Oligocene strata from CIROS-1 drillhole, McMurdo Sound, Antarctica. *Terra Antarctica* **4**, 73–78 (1997).
59. Wilson, G. S., Roberts, A. P., Verosub, K. L., Florindo, F. & Sagnotti, L. Magnetobiostratigraphic chronology of the Eocene–Oligocene transition in the CIROS-1 core, Victoria Land margin, Antarctica: implications for Antarctic glacial history. *GSA Bull.* **110**, 35–47 (1998).
60. Clowes, C. D., Hannah, M. J., Wilson, G. J. & Wrenn, J. H. Marine palynostratigraphy and new species from the Cape Roberts drill-holes, Victoria Land Basin, Antarctica. *Mar. Micropaleontol.* **126**, 65–84 (2016).
61. Houben, A. J. P., Bijl, P. K., Guerstein, G. R., Sluijs, A. & Brinkhuis, H. *Malvinia escutiana*, a new biostratigraphically important Oligocene dinoflagellate cyst from the Southern Ocean. *Rev. Palaeobot. Palynol.* **165**, 175–182 (2011).
62. Houben, A. J. P. et al. Reorganization of Southern Ocean plankton ecosystem at the onset of Antarctic glaciation. *Science* **340**, 341–344 (2013).
63. Ogg, J. G. in *The Geologic Time Scale* (eds Gradstein, F. M. et al.) 85–113 (Elsevier, 2012); https://doi.org/10.1016/B978-0-444-59425-9.00005-6
64. Prebble, J. G., Raine, J. I., Barrett, P. J. & Hannah, M. J. Vegetation and climate from two Oligocene glacioeustatic sedimentary cycles (31 and 24 Ma) cored by the Cape Roberts Project, Victoria Land Basin, Antarctica. *Palaeogeogr. Palaeoclimatol. Palaeoecol.* **231**, 41–57 (2006).
65. Truswell, E. M. & Drewry, D. J. Distribution and provenance of recycled palynomorphs in surficial sediments of the Ross Sea, Antarctica. *Mar. Geol.* **59**, 187–214 (1984).
66. Watkins, D. K., Wise, S. W. & Villa, G. Calcareous nannofossils from Cape Roberts Project drillhole CRP-3, Victoria Land Basin, Antarctica. *Terra Antarctica* **8**, 339–346 (2001).
67. Galeotti, S. et al. Cyclochronology of the Eocene–Oligocene transition from the Cape Roberts Project-3 core, Victoria Land Basin, Antarctica. *Palaeogeogr. Palaeoclimatol. Palaeoecol.* **335–336**, 84–94 (2012).
68. Hayes, D. E., et al. *Initial Reports of the Deep Sea Drilling Project* (US Government Printing Office, 1975).
69. Florindo, F., Wilson, G. S., Roberts, A. P., Sagnotti, L. & Verosub, K. L. Magnetostratigraphic chronology of a late Eocene to early Miocene glacimarine succession from the Victoria Land Basin, Ross Sea, Antarctica. *Glob. Planet. Change* **45**, 207–236 (2005).
70. Naish, T. R., Wilson, G. S., Dunbar, G. B. & Barrett, P. J. Constraining the amplitude of late Oligocene bathymetric changes in western Ross Sea during orbitally-induced oscillations in the East Antarctic Ice Sheet: (2) implications for global sea-level changes. *Palaeogeogr. Palaeoclimatol. Palaeoecol.* **260**, 66–76 (2008).
71. Kim, J.-H. et al. Holocene subsurface temperature variability in the eastern Antarctic continental margin. *Geophys. Res. Lett.* **39**, L06705 (2012).
72. Fielding, C. R. et al. Sequence stratigraphy of the ANDRILL AND-2A drillcore, Antarctica: a long-term, ice-proximal record of early to mid-Miocene climate, sea-level and glacial dynamism. *Palaeogeogr. Palaeoclimatol. Palaeoecol.* **305**, 337–351 (2011).
73. Passchier, S. et al. Early and middle Miocene Antarctic glacial history from the sedimentary facies distribution in the AND-2A drill hole, Ross Sea, Antarctica. *GSA Bull.* https://doi.org/10.1130/B30334.1 (2011).
74. Crampton, J. S. et al. Southern Ocean phytoplankton turnover in response to stepwise Antarctic cooling over the past 15 million years. *Proc. Natl Acad. Sci. USA* **113**, 6868–6873 (2016).
75. Schouten, S., Huguet, C., Hopmans, E. C., Kienhuis, M. V. M. & Sinninghe Damsté, J. S. Analytical methodology for TEX86 paleothermometry by high-performance liquid chromatography/atmospheric pressure chemical ionization–mass spectrometry. *Anal. Chem.* **79**, 2940–2944 (2007).
76. Hopmans, E. C. et al. The effect of improved chromatography on GDGT-based palaeoproxies. *Org. Geochem.* **93**, 1–6 (2016).
77. Schouten, S. et al. An interlaboratory study of TEX86 and BIT analysis of sediments, extracts, and standard mixtures. *Geochem. Geophys. Geosyst.* **14**, 5263–5285 (2013).
78. Kim, J.-H. et al. New indices and calibrations derived from the distribution of crenarchaeal isoprenoid tetraether lipids: implications for past sea surface temperature reconstructions. *Geochim. Cosmochim. Acta* **74**, 4639–4654 (2010).
79. Masson-Delmotte, V. et al. in *Climate Change 2013: The Physical Science Basis* (eds Stocker, T. F. et al.) 383–464 (Cambridge Univ. Press, 2013).
80. Sosdian, S. M. et al. Constraining the evolution of Neogene ocean carbonate chemistry using the boron isotope pH proxy. *Earth Planet. Sci. Lett.* **498**, 362–376 (2018).
81. Martínez-Botí, M. A. et al. Plio–Pleistocene climate sensitivity evaluated using high-resolution CO_2 records. *Nature* **518**, 49–54 (2015).
82. Greenop, R., Foster, G. L., Wilson, P. A. & Lear, C. H. Middle Miocene climate instability associated with high-amplitude CO_2 variability. *Paleoceanography* **29**, 845–853 (2014).
83. Badger, M. P. S. et al. Insensitivity of alkenone carbon isotopes to atmospheric CO_2 at low to moderate CO_2 levels. *Clim. Past* **15**, 539–554 (2019).
84. Mejía, L. M. et al. A diatom record of CO_2 decline since the late Miocene. *Earth Planet. Sci. Lett.* **479**, 18–33 (2017).
85. Super, J. R. et al. North Atlantic temperature and p_{CO_2} coupling in the early–middle Miocene. *Geology* **46**, 519–522 (2018).
86. Witkowski, C. R., Weijers, J. W. H., Blais, B., Schouten, S. & Damsté, J. S. S. Molecular fossils from phytoplankton reveal secular p_{CO_2} trend over the Phanerozoic. *Sci. Adv.* https://doi.org/10.1126/sciadv.aat4556 (2018).
87. Meyers, S., Malinverno, A., Hinnov, L., Zeeden, C. & Moron, V. *astrochron: A Computational Tool for Astrochronology* (2019).

88. Wilson, D. S., Pollard, D., DeConto, R. M., Jamieson, S. S. R. & Luyendyk, B. P. Initiation of the West Antarctic Ice Sheet and estimates of total Antarctic ice volume in the earliest Oligocene. *Geophys. Res. Lett.* **40**, 4305–4309 (2013).
89. DeConto, R. M. et al. Thresholds for Cenozoic bipolar glaciation. *Nature* **455**, 652–656 (2008).
90. Duncan, B. et al. Glycerol dialkyl glycerol tetraether (GDGT) abundances, age–depth tie points and biostratigraphic age events for McMurdo erratics, CIROS-1, CRP-2/2 A, DSDP 270, DSDP 274, ANDRILL 2 A, ANDRILL 1B. *PANGAEA* https://doi.org/10.1594/PANGAEA.946801 (2022).

Acknowledgements

The authors are grateful for access to samples from the IODP core repository at Texas A&M University for DSDP Sites 270 and 274 and to the Alfred Wegener Institute for access to samples from the Cape Roberts Project. This study was funded via an Antarctica New Zealand Sir Robin Irvine PhD Scholarship, Scientific Committee of Antarctic Research Fellowship and Rutherford Foundation Postdoctoral Fellowship (RFT-VUW1804-PD) awarded to B.D., with additional funding by the Royal Society Te Apārangi Marsden Fund award MFP-VUW1808 (B.D. and R.M.) and the New Zealand Ministry of Business Innovation and Employment through the Antarctic Science Platform (ANTA1801) and contract C05X1001 (B.D., R.M., R.L., T.N. and J.G.P.). The Natural Environment Research Council funded J.B. (standard grant Ne/I00646X/1). J.B. and T.D.J. also acknowledge support from Natural Environment Research Council grant NE/P013112/1. D.K.K. was supported by US National Science Foundation award OCE-1326927. The authors are grateful for support from IODP and support in kind from the University of Birmingham and Yale University. We thank S. Schouten (NIOZ) for laboratory support and assistance with temperature data and J. Super for assistance with sample analysis while at Yale University.

Author contributions

B.D, R.M., J.B., R.L. and T.N. designed the research. B.D. processed samples for DSDP 270, DSDP 274 and CRP-2/2A. S.K. conducted analysis on DSDP 270, DSDP 274 and CRP-2/2A. F.S. processed samples and conducted analysis on AND-2A. F.H. processed samples and conducted analysis on additional samples for DSDP 274. V.W. processed samples and conducted analysis on AND-1B, CIROS-1 and the McMurdo Erratics. C.W. processed samples and conducted analysis on AND-1B. J.G.P. and C.C. developed the age model for CIROS-1. S.R.M. contributed statistical analyses. E.G. provided ice-volume model output and advised on interpretation. T.D.J. assisted with temperature calibration interpretations. D.K.K. and C.K. assisted with sedimentological and environmental interpretations for DSDP 270. H.M. advised on laboratory processing and data interpretation. G.T.V. advised on GDGT data interpretation. B.D. created the figures and wrote the text with assistance from all authors, in particular R.M., J.B., R.L. and T.N.

Competing interests

The authors declare no competing interests.

Additional information

Extended data is available for this paper at https://doi.org/10.1038/s41561-022-01025-x.

Supplementary information The online version contains supplementary material available at https://doi.org/10.1038/s41561-022-01025-x.

Correspondence and requests for materials should be addressed to B. Duncan.

Peer review information *Nature Geoscience* thanks the anonymous reviewers for their contribution to the peer review of this work. Primary Handling Editor: Tom Richardson, in collaboration with the *Nature Geoscience* team.

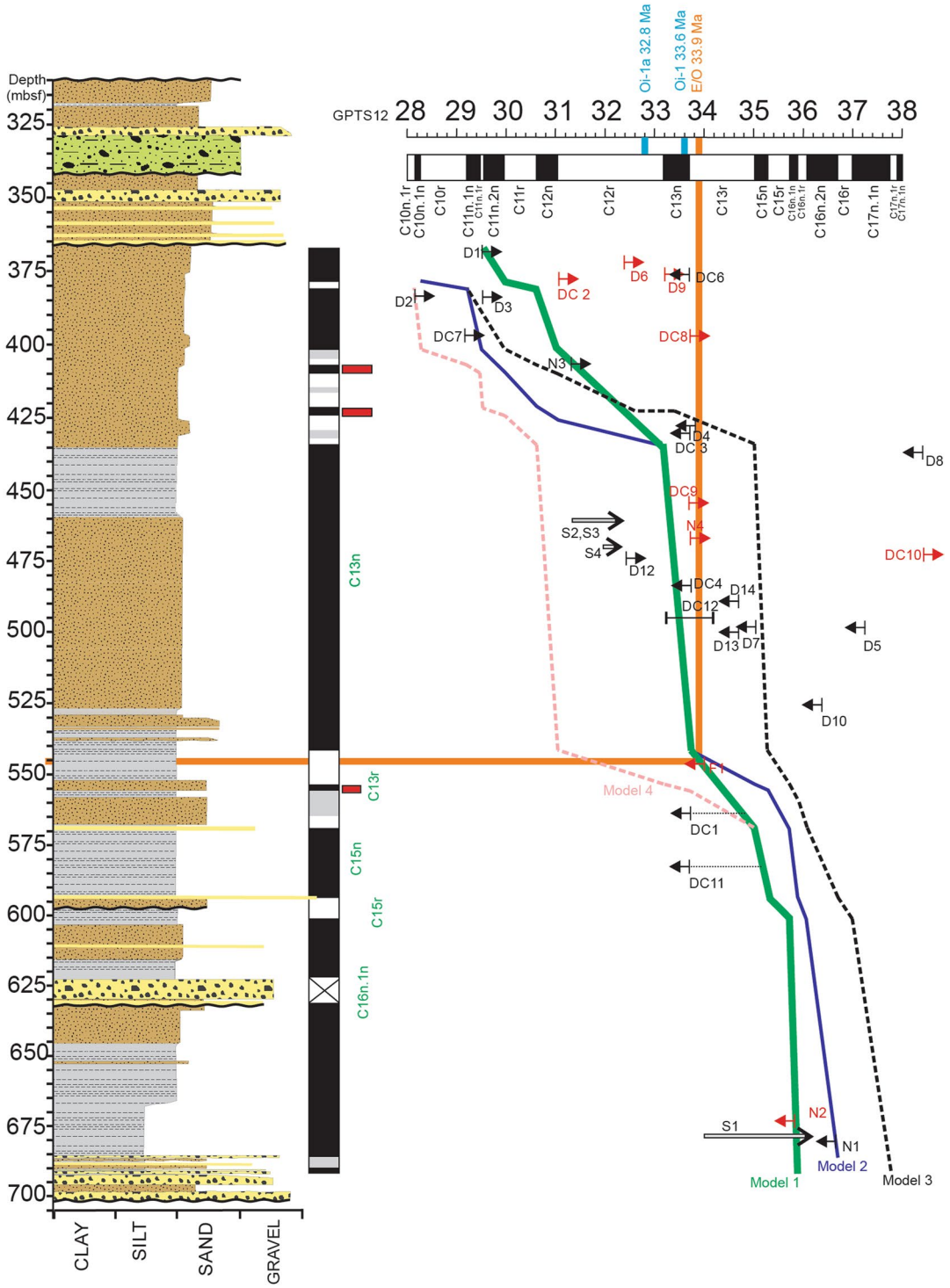

Extended Data Fig. 1 | Age model for CIROS-1. Age model for CIROS-1, based on the paleo-magnetic record from Wilson et al. (1998)[59] and new biostratigraphic events described in Supplementary Data Table 1. The preferred age model is shown in green (model 1), as described in Methods section.